ACS APPLIED MATERIALS & INTERFACES

Research Article

www.acsami.org

# Physiologically Responsive, Mechanically Adaptive Bio-Nanocomposites for Biomedical Applications

Mehdi Jorfi, Matthew N. Roberts, E. Johan Foster, and Christoph Weder*

Adolphe Merkle Institute and Fribourg Center for Nanomaterials, University of Fribourg, Rte de l'Ancienne Papeterie, CH-1723 Marly, Switzerland

Supporting Information

**ABSTRACT:** We report mechanically adaptive bionanocomposites based on poly(vinyl alcohol) (PVOH) and cellulose nanocrystals (CNCs), whose mechanical properties change significantly upon exposure to simulated physiological conditions. These nanocomposites were made using CNCs derived from tunicates (t-CNCs) and cotton (c-CNCs) to explore how aspect ratio, surface charge density, and filler content influence the mechanical properties. Dynamic mechanical analysis data reveal a significant enhancement of the tensile storage modulus ($E'$) upon introduction of CNCs, which scaled with the CNC type and content. For example, in the dry, glassy state at 25 °C, $E'$ increased up to 23% (for c-CNCs) and 88% (for t-CNCs) compared to the neat polymer. Exposing the materials to simulated physiological conditions caused a drastic softening of the materials, from 9.0 GPa to 1 MPa for c-CNCs and from 13.7 GPa to 160 MPa for t-CNCs. The data show that the swelling characteristics of the nanocomposites and the extent of mechanical switching could be influenced via the amount and type of CNCs and also the processing conditions. The high stiffness in the dry state and the ability to tailor the mechanical contrast via composition and processing makes the new materials particularly useful as basis for adaptive biomedical implants.

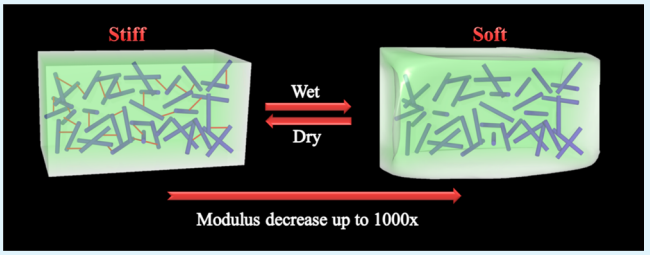


**KEYWORDS:** *cellulose nanocrystals, poly(vinyl alcohol), polymer nanocomposites, mechanically adaptive, responsive*

## INTRODUCTION

Materials that selectively respond to external stimuli are often referred to as "smart", "intelligent", or "adaptive" because of their intrinsic ability to change their physical or chemical properties on command.[1,2] Among many other uses, they have garnered significant attention due to their potential applications in biomedical and biotechnological fields,[3−5] including their use as transient implants,[6,7] drug delivery carriers,[8,9] tissue-engineering scaffolds,[10,11] thermoresponsive hydrogels,[12] self-healing materials,[13,14] cell cultures,[15] bioseparation membranes,[16] sensors, and actuators.[17,18] One intriguing feature exhibited by some of these materials is their ability to change mechanical properties "on command".[19] One recently demonstrated approach for the design of such materials relies on the preparation of polymer-based nanocomposites, which are composed of a polymeric matrix and reinforcing nanofibers, whose interactions are stimuli-responsive and regulate the mechanical properties of the bulk material.[19,20] In a recent study, Korley et al. extended this concept to polymer composites based on electrospun nanofibers as the filler, where mechanical morphing is achieved by changing the properties of the filler and not filler−filler or filler−matrix interactions.[21]

Among many potential nanofillers, crystalline cellulose nanofibers, referred to as "nanowhiskers", have been widely investigated.[22−25] Cellulose nanocrystals (CNCs) can be isolated from a variety of sources, including plants (e.g., wood, cotton, or wheat straw), marine animals (tunicates), as well as bacterial sources, such as algae, fungi, and amoeba (protozoa).[22] Using CNCs isolated from tunicates, Favier et al. reported the first CNC-reinforced polymer nanocomposites in 1995. These materials displayed substantially enhanced mechanical properties, which were explained with the formation of a percolating, hydrogen-bonded network of CNCs within the polymer matrix.[26,27] This initial work was followed by a large number of studies that explored the reinforcement of a plethora of polymer matrices with CNC from a broad range of sources.[19,20,22,25] The widespread interest in CNC-based nanocomposites is explained by the low cost, outstanding mechanical properties, availability, sustainability, biodegradability, and low density of CNCs.

In a series of contributions, we demonstrated that the stiffness of CNC-based nanocomposites can be reversibly changed by controlling the degree of interactions between the rigid filler.[20,28−33] The CNCs form a percolating network within the matrix that is, among several contributing intermolecular forces, primarily held together by hydrogen-bonds among the surface hydroxyl groups, although CNC-

Received: December 18, 2012
Accepted: February 4, 2013
Published: February 4, 2013

   dx.doi.org/10.1021/am303160j | ACS Appl. Mater. Interfaces 2013, 5, 1517−1526

polymer interactions may also play an important role.[34−36] This causes a significant reinforcement of the polymer matrix. Upon exposure to chemicals that can competitively hydrogen-bond to the CNCs or interfere with intermolecular van der Waals forces, for example, water, the interactions between individual CNCs are reduced and the nanocomposite softens considerably, as predicted by mechanical models. Our first generation of such mechanically adaptive nanocomposites was based on a rubbery ethylene oxide-epichlorohydrin copolymer (EO-EPI) and t-CNCs.[28,37] Incorporation of 19% v/v t-CNCs into EO-EPI results in an increase of the storage modulus, $E'$, from 3.7 MPa (neat EO-EPI) to 800 MPa (EO-EPI/t-CNC nanocomposite) at 25 °C. These materials undergo a pronounced and reversible modulus reduction from 800 to 20 MPa upon exposure to water. Plasticization of the polymer matrix upon aqueous swelling has been shown to reinforce the effect, for example in nanocomposites based on poly(vinyl acetate) (PVAc) and t-CNCs or c-CNCs.[29,30] The PVAc/t-CNC nanocomposites showed an increase of the $E'$ from 1.8 GPa (neat PVAc) to 5.2 GPa for a nanocomposite containing 16.5% v/v t-CNCs. Because of the glassy nature of the PVAc matrix, these materials exhibit a much higher initial stiffness than the EO-EPI-based systems, but soften greatly (5.2 GPa to 12 MPa) upon exposure to water due to matrix plasticization and t-CNCs decoupling.

We have shown that such biologically inspired mechanically adaptive materials are potentially useful as substrates for medical devices, for example intracortical microelectrodes.[38,39] Such neural prosthetic devices, which connect the brain with the outside world, promise to be useful for many clinical applications, but it has proven difficult to achieve long-term connectivity, presumably on account of the mechanical-mismatch between current electrode materials and the cortical tissue.[40] Initial in vivo experiments with PVAc/t-CNC nanocomposites suggest that mechanically adaptive intracortical neural prosthetics can more rapidly stabilize neural cell populations at the interface than rigid systems, which bodes well for improving the functionality of intracortical devices.[39,41] The realization of such intracortical electrodes,[38] and other medical devices would benefit significantly, if mechanically adaptive materials with a higher than currently available stiffness ($E'$ = 5.2 GPa)[30] could be made available. Thus, we have explored mechanically adaptive stimuli-responsive nanocomposites based on PVOH as the matrix and CNCs derived from tunicates (t-CNCs) and cotton (c-CNCs) as the filler. This design was based on the hypothesis that the use of a polar glassy polymer that promotes significant matrix-CNC interactions would result in stiffer nanocomposites than previously employed matrices. With this perspective, PVOH was chosen for this purpose because it can be water-soluble (depending on the degree of hydrolysis and heat treatment)[42] and has many hydroxyl groups that can interact with the surface hydroxyls of CNCs. Moreover, PVOH is biocompatible, nontoxic, and already used in a wide variety of biomedical applications, such as contact lenses[43−45] and FDA-approved nerve grafts.[46] Several studies have reported PVOH-based nanocomposites with t-CNCs[47] and c-CNCs,[48−50] as well as microfibrillated cellulose.[51] While previous work has shown dynamic mechanical properties of such nanocomposites by exposing them to humid atmosphere, we herein investigate the dynamic mechanical properties by complete submersion into a simulated physiological fluid to explore the properties under more relevant conditions for use in biomedical applications. We demonstrate that by particular processing conditions, it is possible to control the aqueous swelling of the material and the degree of softening it experiences.

## EXPERIMENTAL SECTION

**Materials.** Poly(vinyl alcohol) (PVOH) 99% hydrolyzed ($M_w$ = 85 000−124 000 g/mol; $\delta$ = 1.26 g/mL) and all reagents were purchased from Sigma-Aldrich and used without further purification. Artificial cerebrospinal fluid (ACSF) was prepared by dissolving the following materials in 1 L of deionized water: NaCl = 7.25 g, KCl = 0.22 g, $NaHCO_3$ = 2.18 g, $CaCl_2{\cdot}2H_2O$ = 0.29 g, $KH_2PO_4$ = 0.17 g, $MgSO_4{\cdot}7H_2O$ = 0.25 g, and D-glucose =1.80 g.[52] A literature value of 1.46 g/mL was used for the density of the CNCs.[53]

**Isolation of Cellulose Nanocrystals from Tunicates.** t-CNCs were isolated from tunicates (*Styela clava*) collected from floating docks in Point View Marina (Narragansett, RI). The t-CNCs were prepared by sulfuric acid hydrolysis of the cellulose pulp. The protocol was based on the method described by Favier et al.,[26] utilized modifications reported by Shanmuganathan et al.,[30] and relied on minor changes that are detailed in the Supporting Information.

**Isolation of Cellulose Nanocrystals from Cotton.** c-CNCs were isolated from Whatman filter paper with minor modifications to a previously published procedure.[54] After sulfuric acid hydrolysis and dialysis treatment, the resulting dispersion was sonicated for 3 h and left to settle at room temperature for 18 h. The supernatant was then decanted off and the c-CNC dispersion was spray-dried using a Büchi Mini Spray Dryer (Model B-191) to yield dried c-CNCs as a white powder. The drying parameters were an inlet temperature of 110 °C, a flow rate of 4 mL/min, a nozzle airflow of 700 mL/min, an aspiration rate of 70%, and an outlet temperature of 60 °C.

**Preparation of PVOH/CNC Nanocomposites.** Lyophilized t-CNCs or spray-dried c-CNCs were dispersed in deionized water at a concentration of 5 mg/mL by sonicating for 10 and 7 h, respectively. PVOH was dissolved in deionized water at a concentration of 50 mg/mL by stirring for 2 h at 90 °C. Nanocomposites comprising 4−16% v/v CNCs were prepared by combining the appropriate amounts of the CNC dispersion and PVOH solution to cast a film weighing 1 g. This mixture was stirred at room temperature for 30 min, followed by sonication for 30 min, and the resulting homogeneous mixtures were cast into Teflon Petri dishes of a diameter of 100 mm. The dishes were placed into an oven at 35 °C for 5 days to evaporate the water, and the resulting films were then further dried in the oven at 70 °C for 24 h. The films were compression-molded between spacers in a Carver laboratory press (1000 psi for 2 min, followed by an increase of pressure to 2000 psi for 15 min). Unless otherwise stated, PVOH/t-CNC films were compression-molded at 150 °C, and PVOH/c-CNC films were compression molded at 120 °C. Both types of films were allowed to cool to ∼70 °C over the course of ∼90 min under the applied pressure to yield 70−100 $\mu$m thin nanocomposite films. The thickness of the films was measured using an electronic digital caliper (Fowler) and micrometer (Millimess Inductive Digital Comparator Extramess 200, Mahr). For reference purposes, neat PVOH films were prepared in a similar manner by solution-casting and subsequent compression-molding at 120 and 150 °C.

**Atomic Force Microscopy (AFM).** Atomic force microscopy was carried out on a NanoWizard II (JPK Instruments) microscope. Ten microliters of dilute aqueous CNC dispersions (0.1 mg/mL) were deposited onto freshly cleaved mica (SPI Supplies Division of Structure Probe, Inc.) and allowed to dry at 70 °C for 2 h. The scans were performed in tapping mode in air using silicon cantilevers (NANO WORLD, TESPA-50) with a scan rate of 1 line/sec.

**Transmission Electron Microscopy (TEM).** The dimensions of the CNCs were examined by transmission electron microscopy (TEM) using a Hitachi H-1700 microscope operating at an accelerating voltage of 75 kV. To assess the CNCs dimensions, lyophilized CNCs were dispersed in deionized water at a concentration of 0.1 mg/mL by sonication. Subsequently, 3 $\mu$L of the aqueous CNC dispersions were deposited on carbon-coated grids (Electron Microscopy Sciences) and allowed to dry at 70 °C for 2 h.

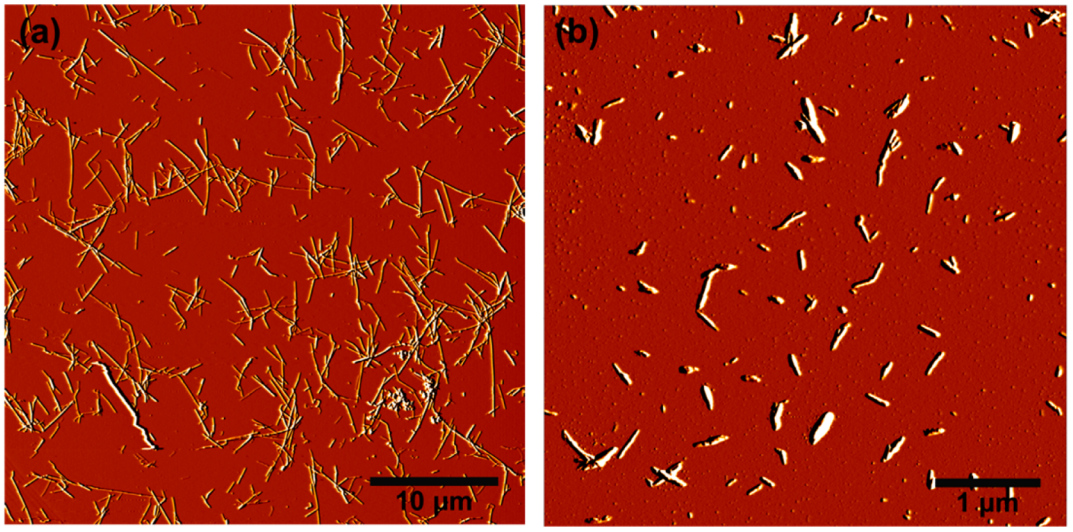


**Figure 1.** AFM amplitude images for (a) lyophilized t-CNCs and (b) spray-dried c-CNCs deposited from aqueous dispersions (0.1 mg/mL) onto freshly cleaved mica surfaces.

CNC dimensions were determined by analyzing 10 TEM images of CNCs with a total of more than 100 individual CNCs of which length and width were measured. The dimensions thus determined are reported as average values ± standard error.

**Conductometric Titration.** Conductometric titrations were performed to quantify the surface charges of CNCs. 50 mg of the CNCs were suspended into 10−15 mL of aqueous 0.01 M hydrochloric acid. After 5 min of stirring and 30 min of sonication, the suspensions were titrated with 0.01 M NaOH. The titration curves were evaluated by considering the following three regions: the titration of the excess of HCl, a weak acid corresponding to the sulfate-ester surface groups, and finally the excess NaOH present after titration of all of the acid (see Figure S1 in the Supporting Information). The three regions were separately fit to lines, and the volume of NaOH used to titrate the sulfate-ester groups was determined by the volume comprised within the points at which the linear fits intersect one another (shown graphically in Supporting Information Figure S1). To assess the accuracy of this titration volume with regard to other weakly acidic species being in solution, such as dissolved $CO_2$, a blank titration was performed without CNCs present in solution. This volume was calculated to be 0.08 mL of NaOH and was subtracted from the volumes determined for titrations containing CNCs to further calculate the sulfate charge density. The concentration of sulfate groups was calculated by

$$\frac{\text{mmol of } SO_4^-}{\text{kg of cellulose}} = \frac{C_{NaOH} \times V_{NaOH}}{W_{CNC}} \times 10^6 \quad (1)$$

where $C_{NaOH}$ is the concentration of the base (0.01 M), $V_{NaOH}$ is the volume (L) of NaOH used to titrate the weak acid, and $W_{CNC}$ is the weight of S-CNCs employed for the measurement (g).

**Swelling Behavior.** The swelling behavior of the PVOH/CNC nanocomposites was investigated by immersing the materials in artificial cerebrospinal fluid (ACSF) at human body temperature (37 °C) over the course of 2 months. The degree of swelling was determined by measuring the weight of the samples pre- and postswelling:

$$\text{degree of swelling (\%)} = \frac{\text{mass of wet sample} - \text{mass of dry sample}}{\text{mass of dry sample}} \times 100 \quad (2)$$

To minimize the error in measuring the degree of swelling, once the wet samples were taken out of the ACSF, they were placed on paper tissue to wick any excess ACSF from the surface; the samples were then immediately weighed.

**Dynamic Mechanical Analysis (DMA).** The mechanical properties of the PVOH/CNC nanocomposites were characterized by dynamic mechanical analysis (DMA) using a TA Instruments Model Q800. Tests were conducted in tensile mode using a temperature sweep method (0−140 °C) at a fixed frequency of 1 Hz, a strain amplitude of 30 μm, a heating rate of 5 °C/min and a gap distance between the jaws of ∼10 mm. The samples were prepared by cutting strips from the films with a width of ∼6 mm. To determine the mechanical properties of the films in the wet state, the samples were swelled in ACSF at 37 °C for periods of 1 week and 1 month. DMA experiments were conducted in tensile mode with a submersion clamp, which allowed measurements while the samples were immersed in ACSF. In this case, the temperature sweeps were done in the range of 23−75 °C with a heating rate of 1 °C/min, a constant frequency of 1 Hz, a strain amplitude of 30 μm and a fixed gap distance between jaws of 15 mm.

**Stress−Strain Measurements.** Stress−strain measurements of PVOH/CNCs nanocomposites were performed using a TA Instruments Model Q800 dynamic mechanical analyzer. Tests were carried out at 25 °C with a strain rate of 0.5%/min, a preload force of 0.01 N, a gap distance between the jaws of ∼10 mm, and using dog-bone shaped films having a width of 2.1 mm. Tensile moduli were calculated from the slopes of the linear region between 0 and 0.3% strain.

**Differential Scanning Calorimetry (DSC).** Differential scanning calorimetry experiments were carried out with a Mettler Toledo STAR instrument under $N_2$ atmosphere. The typical procedure included heating and cooling cycles of approximately 10 mg sample in a DSC pan from −50 to 250 °C using a heating rate of 10 °C/min. The glass transition temperature ($T_g$) was determined from the midpoint of the specific heat increment at the glass−rubber transition, while the melting temperature ($T_m$) was taken by the highest temperature point of the melting endotherm.

## RESULTS AND DISCUSSION

**Isolation and Physical Properties of Cellulose Nanocrystals.** The CNCs used in this study were isolated from tunicates (t-CNCs) and cotton (c-CNCs) by sulfuric acid hydrolysis, using protocols that represent modified versions of well-established methods. In the case of c-CNCs, spray-drying was used to isolate the dry CNCs (see Experimental Section). Polymer nanocomposites with t-CNCs have consistently been shown to exhibit superior mechanical properties than those with c-CNCs, a fact that is mainly credited to their higher aspect ratio (∼70 vs ∼10),[23,24] and on-axis stiffness (tensile

modulus ~143 vs ~105 GPa).[55,56] c-CNCs, on the other hand, are more viable for commercial exploitation, because they are isolated from an abundant and sustainable biosource. Due to their high density of strongly interacting surface hydroxyl groups, CNCs have a strong tendency for self-association.[37,54,57] Transmission electron microscopy (TEM) and atomic force microscopy (AFM) images of the CNCs confirm that redispersion of the dried materials in water is readily possible (Figure 1, and Supporting Information Figures S2–S4). The dimensions of the t-CNCs, determined from TEM micrographs, were an average length and width of 2500 ± 1000 nm and 30 ± 5 nm, respectively. The average aspect ratio ($A$, defined as length to width ratio, $l/w$) of the t-CNCs is therefore 83. The charge density of negatively charged sulfate esters on the CNC surface that are introduced during hydrolysis has been suggested to modulate CNC–CNC interactions and to affect their dispersibility. By conductometric titration, the density of sulfate groups of the present t-CNCs was determined to be ~75 mmol/kg (Figure S1a in the Supporting Information).

The c-CNCs used here were measured to have an average length and width of 220 ± 70 and 22 ± 6 nm, respectively, resulting in an aspect ratio of 10. In addition to exhibiting a lower aspect ratio than the t-CNCs, the charge density on the surface of c-CNCs (~25 mmol/kg, Figures S1b and S1c in the Supporting Information), is significantly lower than that of t-CNCs. While t-CNCs were dried and isolated by lyophilization, spray-drying was used for c-CNCs. To assess any influence of the drying process on the physical properties of the c-CNCs, one batch of as-prepared c-CNCs was, after dialysis and sonication, split into two portions, which were dried by lyophilization and spray drying, respectively. TEM and conductometric titration data suggest that the drying method has no influence on the physical dimensions of the c-CNCs or on their surface charge density and morphology (Supporting Information Figures S1–S3).

**Nanocomposite Processing.** PVOH solutions and CNC dispersions were combined, and after solution-casting and evaporation of solvent, the resulting films were reshaped by compression-molding to result films of the nanocomposite with 4–16% v/v CNCs and a thickness of 70–100 $\mu$m. Because of the limited thermal stability of the nanocomposites above the melting temperature ($T_m$) of PVOH (~220 °C), the films were compressed at a temperature much below $T_m$. PVOH/t-CNC nanocomposites were compression-molded at 150 °C without any visible color changes, while PVOH/c-CNC nanocomposites yellowed, when processed at this temperature (Figure S5 in the Supporting Information). As a consequence, PVOH/c-CNC nanocomposites were processed at 120 °C, unless otherwise noted. Several explanations have been proposed in the literature regarding the degradation of CNCs,[58–60] and we speculate the differences in thermal degradation arise from differences related to the source of CNCs.

**Thermal Properties.** The thermal properties of PVOH/CNC nanocomposites were determined using differential scanning calorimetry (DSC, Table 1). The DSC curves (Figure S6 in the Supporting Information) show that the $T_g$ (68 and 71 °C) and $T_m$ (216 and 217 °C) of the neat PVOH only slightly depends on the temperature at which the films were compression-molded. In both cases, the incorporation of CNCs led to an increase of $T_g$ by approximately 10 °C, which interestingly was independent of the CNC content. The $T_g$ of the polymer nanocomposites is strongly influenced by the extent of interactions between nanoparticles and polymer chains.[61] In the present work, both the polymer matrix and reinforcing phase are rather hydrophilic. Hence, strong molecular interactions (hydrogen bonding or van der Waals forces) between the polymer and CNCs can be expected, which can restrict the segmental mobility of the macromolecules and thereby increase $T_g$. A similar trend was found in PVOH-based nanocomposites, comprising CNCs,[50] bacterial cellulose nanocrystals,[62] or nanoclay particles.[63] In addition, upon introduction of CNCs, the width of the melting peak increases, and the degree of crystallinity ($\chi_c$) increases slightly. This shows that the CNCs perhaps act as small nucleation sites for the crystallization of PVOH. Also this effect was largely independent of the CNC content.

**Table 1. Thermal Properties of Neat PVOH and PVOH/CNC Nanocomposites as a Function of CNC Type and Content**

| sample | CNC content (% v/v) | $T_g$ (°C)[a] | $T_m$ (°C)[a] | $\Delta H_m$ (J/g) | $\chi_c$ (%)[b] |
|---|---|---|---|---|---|
| neat PVOH[c] | | 71 | 217 | 43.9 | 27 |
| PVOH/t-CNC | 4 | 81 | 218 | 50.2 | 33 |
| | 8 | 83 | 214 | 49.7 | 34 |
| | 12 | 82 | 220 | 48.8 | 35 |
| | 16 | 82 | 215 | 44.1 | 34 |
| neat PVOH[d] | | 68 | 216 | 49.6 | 31 |
| PVOH/c-CNC | 4 | 79 | 216 | 58.5 | 38 |
| | 8 | 80 | 213 | 52.4 | 36 |
| | 12 | 81 | 212 | 47.3 | 34 |
| | 16 | 82 | 210 | 40.9 | 31 |

[a]The data obtained from the second heating scan of DSC measurements. [b]$\chi_c = (\Delta H_m)/(w\Delta H_0)$, where $w$ is the weight fraction of polymer matrix in the nanocomposites, $\Delta H_m$ is the measured melting enthalpy and $\Delta H_0$ is the enthalpy of 100% crystalline PVOH (161 J/g).[73] [c]Films were compression-molded at 150 °C. [d]Films were compression-molded at 120 °C.

**Mechanical Properties of Dry PVOH/CNC Nanocomposites.** The mechanical properties of the nanocomposites were established using dynamic mechanical analysis (DMA, Table 2). Figure 2a shows the tensile storage moduli ($E'$) of the PVOH/t-CNC nanocomposites and a neat PVOH reference film in the dry state as a function of temperature. At room temperature (25 °C), the neat PVOH matrix, processed at 150 °C exhibits an $E'$ of 7.3 GPa. Upon increasing the temperature, $E'$ drastically decreases to 840 MPa at 100 °C (~$T_g$ + 30 °C) due to a transition from the glassy to the rubbery regime at ~70 °C, which is seen as a maximum in the tan $\delta$ curves (Figure 2b). PVOH/t-CNC nanocomposites containing 4 to 16% v/v t-CNCs showed a significant increase in $E'$ compared to the neat matrix below and above the $T_g$. At 25 °C, $E'$ increased from 7.3 GPa (neat PVOH) to 13.7 GPa for the nanocomposite containing 16% v/v t-CNCs (Figure 2a and Table 2). A more significant reinforcement was observed above $T_g$. At 100 °C, the nanocomposite containing 16% v/v t-CNCs shows an $E'$of 5.4 GPa, which represents a 7-fold increase over the stiffness of the neat PVOH (840 MPa) at this temperature. At temperatures well above $T_g$ where the softening of the material is attributed to higher polymer chain mobility, the significantly higher stiffness of the nanocomposites at these temperatures supports the notion that a percolating network of stiff CNCs reinforces the surrounding soft polymer matrix. Theoretically, further

**Table 2. Tensile Storage Moduli ($E'$) of Dry and ACSF-Swollen Films of Neat PVOH and PVOH/CNC Nanocomposites Determined by DMA[a]**

| | | dry nanocomposites | | swollen nanocomposites | |
|---|---|---|---|---|---|
| sample | CNC content (% v/v) | $E'$ at 25 °C (GPa) | $E'$ at 100 °C (GPa) | $E'$ at 37 °C after 1 week in ACSF (MPa) | $E'$ at 37 °C after 1 month in ACSF (MPa) |
| Neat PVOH[b] | | 7.3 | 0.84 | 11.1 | 6.9 |
| PVOH/t-CNC | 4 | 10.5 | 2.1 | 45.4 | 46.8 |
| | 8 | 11.1 | 3.7 | 78.3 | 85.2 |
| | 12 | 11.7 | 4.7 | 124 | 108 |
| | 16 | 13.7 | 5.4 | 164 | 173 |
| | 16[c] | 12.3 | 3.0 | 60[d] | n.m. |
| Neat PVOH[c] | | 7.0 | 0.7 | 1.4[d] | n.m. |
| PVOH/c-CNC | 4 | 6.8 | 0.5 | 1.5[d] | n.m. |
| | 8 | 7.7 | 0.8 | 3.6[d] | n.m. |
| | 12 | 8.3 | 1.0 | 1.6[d] | n.m. |
| | 16 | 9.0 | 1.4 | 1.9[d] | n.m. |
| | 16[b] | 8.4 | 2.1 | 13[d] | n.m. |

[a]Data represent averages ($N$ = 4–7). [b]Films were compression-molded at 150 °C. [c]Films were compression-molded at 120 °C. [d]Samples were measured after 1 day immersed in ACSF. n.m. = not measured.

reinforcement is possible with higher loadings, although practical limitations regarding the brittleness of the material make 16% v/v loading a reasonable upper limit.

The $E'$ of nanocomposites prepared with c-CNCs exhibits a similar trend as observed for the t-CNC nanocomposites, although the stiffness increase was more modest. As discussed above, PVOH/c-CNC nanocomposite films yellowed upon compression molding at 150 °C and were thus processed at 120 °C. At all temperatures, the $E'$ of dry PVOH reference films, processed at 120 °C, was found to be slightly lower than that of the neat PVOH processed at 150 °C (Figure 2a, 2c, and Table 2). For example, at 25 °C $E'$ values of 7.3 and 7.0 GPa were measured. PVOH/c-CNC nanocomposite with 16% v/v c-CNCs exhibited a $E'$ of 9.0 GPa at 25 °C, which is higher than that of the neat PVOH (7.0 GPa), but lower than the $E'$ of 13.7 GPa of the t-CNC nanocomposite with the same CNC content. Above $T_g$ (at 100 °C) $E'$ of this nanocomposite was 1.4 GPa, which represent a 2-fold enhancement over the stiffness of the neat polymer (Figure 2c and Table 2). The lower reinforcement displayed by the c-CNCs compared to the t-CNCs is consistent with previous findings and can be attributed to lower aspect ratio and stiffness of c-CNCs.[20]

Figure 2b and 2d displays the loss factor (tan $\delta$) curves of neat PVOH and the two series of nanocomposites as a function of temperature. Tan $\delta$ is the ratio of loss modulus to storage modulus $E''/E'$ of the material and is indicative of its damping behavior. All curves show a single relaxation peak centered at $T_\alpha$, which corresponds to the $T_g$ determined by DSC. The introduction of CNCs led to a reduction in peak intensity ($I_\alpha$) and a shift of $T_\alpha$ to higher temperature compared to the neat PVOH films. The peak intensity of the curve is indicative of the magnitude of energy loss because of relaxation processes in the material, which in this case reflect polymer chain relaxation due to the onset of the glass transition. The trend of decreasing $I_\alpha$ and increasing $T_\alpha$ is attributed to the reduced mobility of PVOH chains in the amorphous phase due to the presence of the CNCs, but it is, unfortunately, not possible to deduce to what extent CNC−CNC or CNC−PVOH interactions contribute to this effect. Above a CNC content of 8% v/v, that is, in a regime where the CNC concentration is above the percolation threshold, the changes in $I_\alpha$ and $T_\alpha$ seem to level off.

Table 3 shows a comparison of the $E'$ values of the dry PVOH/CNC nanocomposites studied here with previously reported mechanically adaptive nanocomposites based on a range of polymer matrices. The data are quoted for a filler content of ∼16% v/v. The comparison shows that the stiffness of the present PVOH/t-CNC nanocomposites at 25 °C is more than three times higher than that of the stiffest mechanically adaptive nanocomposites reported to date. This implies that a good dispersion of the CNCs has been achieved in the PVOH matrix and supports the conclusion that strong molecular interactions such as H-bonding[50] or van der Waals forces[64] between the CNCs and the polymer matrix indeed increase the reinforcing effect of the cellulose. Similar observations have been reported for other PVOH-based nanocomposites with strong polymer−filler interactions.[50,65,66]

To further evaluate the reinforcing effect of the CNCs on the mechanical properties of the nanocomposites, the Young's moduli of the nanocomposites with 8 and 16% v/v CNC content were determined by way of tensile testing (Supporting Information Figure S7). The Young's modulus changed in a similar manner as $E'$ (i.e, from 12.2 GPa for the neat PVOH to 15.3 and 17.1 GPa for nanocomposites with 8 and 16% v/v t-CNC and to 13.8 and 15.5 GPa for nanocomposites with 8 and 16% v/v c-CNC). The maximum stress increased from 104 MPa for the neat PVOH to 130 and 140 MPa for nanocomposites with 8 and 16% v/v t-CNC and to 126 and 110 MPa for nanocomposites with 8 and 16% v/v c-CNC.

**Analysis of Mechanical Data in the Framework of the Percolation Model.** The mechanical reinforcement in optimally assembled CNC nanocomposites is caused by the formation of a percolating CNC network, in which stress transfer is facilitated by intermolecular interactions between the CNCs.[26] The stiffness of these materials can be described by a percolation model that has been successfully used to predict the mechanical behavior of heterogeneous materials, such as polymer blends[67] and nanocomposites.[28−30,37,68] Detailed information about the percolation model and its use for modeling CNCs-based nanocomposites can be found elsewhere.[25] Within the framework of this model, $E'$ of the nanocomposite can be expressed by

$$E' = \frac{(1 - 2\psi + \psi X_r)E'_s E'_r + (1 - X_r)\psi E'^2_r}{(1 - X_r)E'_r + (X_r - \psi)E'_s} \quad (3)$$

The subscripts s and r refer to the soft phase (polymer matrix) and rigid phase (CNCs), respectively. $\psi$ is the volume fraction of the percolating rigid phase (CNCs) that participates in the load transfer, which can be written as

$$\psi = X_r\left(\frac{X_r - X_C}{1 - X_C}\right)^{0.4} \quad (4)$$

where $X_r \geq X_C$; $X_r$ is the volume fraction of CNCs and $X_C$ is the critical CNC volume fraction (percolation threshold), which was calculated by $0.7/A$. Figure 3a and 3b show the predictions for the two series of nanocomposites studied here, along with experimentally determined $E'$ values of dry PVOH/CNC

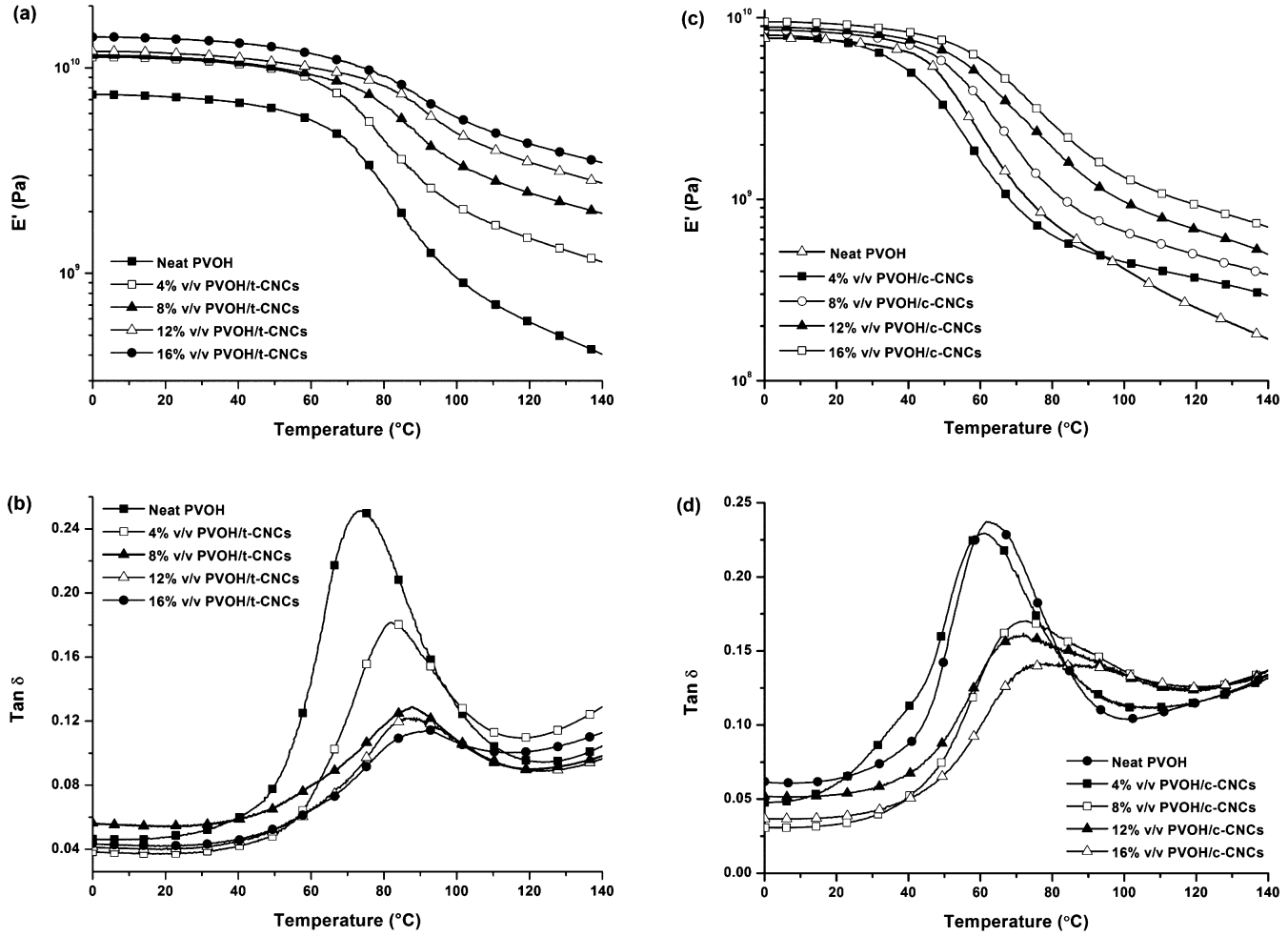


**Figure 2.** Dynamic mechanical analysis (DMA) data of dry PVOH and dry PVOH/CNC nanocomposites as a function of temperature and CNC content. (a) Tensile storage moduli ($E'$) and (b) loss tangent (tan $\delta$) of PVOH/t-CNC nanocomposites. (c) Tensile storage moduli ($E'$) and (d) loss tangent (tan $\delta$) of PVOH/c-CNC nanocomposites.

**Table 3. Comparison of Tensile Storage Moduli ($E'$) of Current Materials with Previous Mechanically Adaptive Nanocomposites Comprising ~16% v/v of CNCs**

| CNC type | polymer matrix | $E'$ of neat polymer at 25 °C (GPa) | $E'$ of nanocomposite at 25 °C (GPa) | ref |
|---|---|---|---|---|
| tunicate | EO-EPI | 0.004 | 0.8 | 28 |
| tunicate | PBMA | 0.6 | 3.8 | 20 |
| tunicate | PVAc | 2.0 | 5.2 | 20 |
| cotton | PVAc | 2.0 | 4.0 | 29 |
| tunicate | PVOH | 7.3[a] | 13.7 | this work |
| cotton | PVOH | 7.0[b] | 9.0 | this work |

[a]PVOH film was compression-molded at 150 °C. [b]PVOH film was compression-molded at 120 °C.

nanocomposites at 100 °C, that is, at ~$T_g$ + 30 °C. For the calculations, aspect ratios ($A$) of 83 and 10 (as determined by TEM) were used for t-CNCs and c-CNCs, respectively, and storage moduli $E'_S$ of 840 MPa (for the PVOH processed at 150 °C) and 700 MPa (for the PVOH processed at 120 °C) were employed for the neat polymer matrix at 100 °C (as determined by DMA). The tensile storage modulus of the CNC phase, $E'_r$, was in previous studies derived by either measuring the stiffness of a neat t-CNC or c-CNC film or by fitting the model against the experimentally determined properties of the nanocomposites and using $E'_r$ as a fit parameter. While the morphology (and therewith the stiffness) of a neat CNCs film depends strongly on the processing conditions and has little resemblance to that of a CNC network within a polymer matrix, the $E'_r$ values of 5−24 GPa for t-CNC-based,[28,30,69] and 0.6−5 GPa for c-CNC-based[29,37,69] nanocomposites determined by these approaches appeared to roughly match. Interestingly, $E'_r$ values of 80 and 10 GPa are required to fit the model to the data for the t-CNC-based and c-CNC-based nanocomposites with PVOH studied here (Figures 3a, and 3b). A comparison of the data for several other t-CNC-based nanocomposites shows that for a given CNC content, $E'$ increases with the polarity of the polymer matrix (PS[37] < PVAc[30] < Epoxy[69]), suggesting that systems with pronounced CNC-polymer interactions may exhibit larger reinforcement due to factors that are not explicitly accounted for in the percolation model.[69] This conclusion is consistent with the results of Dufresne and co-workers, who also reported difficulty in fitting data for PVOH/c-CNC nanocomposites according to the methods used for similar materials.[50]

**Swelling Behavior.** The swelling behavior of the nanocomposites in physiological conditions was investigated by immersing the materials into artificial cerebrospinal fluid (ACSF) at 37 °C to mimic physiological conditions. It is known that heat-treated, PVOH is no longer water-soluble,[42]

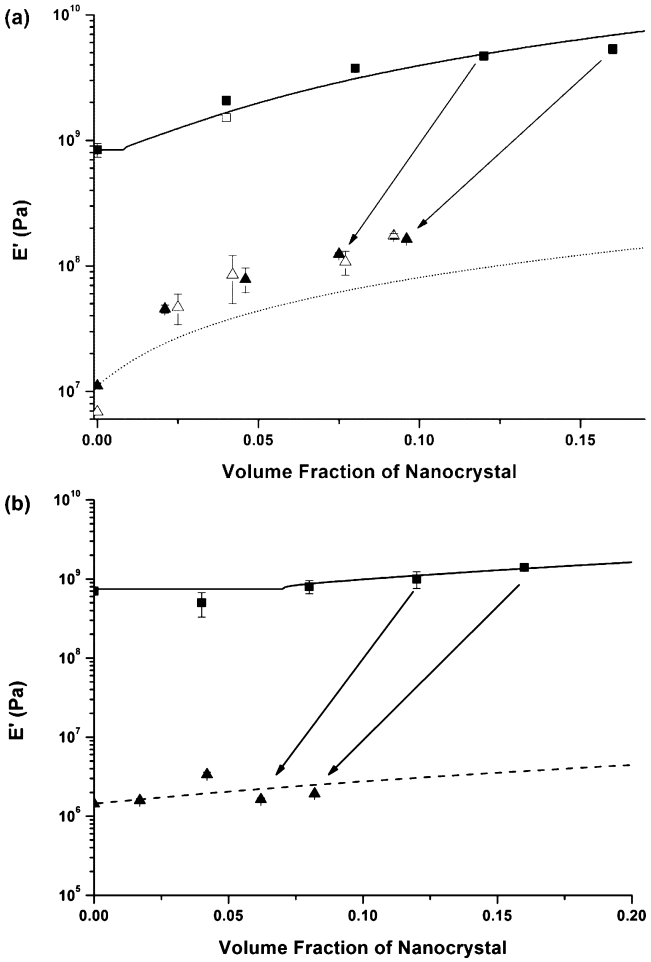


**Figure 3.** (a) Tensile storage moduli ($E'$) of neat PVOH and PVOH/t-CNC nanocomposites as a function of CNC content in the dry state at 100 °C (■), redried after swelling with ACSF for 1 week (□), ACSF-swollen after immersion in ACSF at 37 °C for 1 week (▲), and 1 month (Δ). The solid line shows values predicted by the percolation model for the dry state ($E'_r$ = 80 GPa). The dotted line shows values predicted by the Halpin−Kardos model for samples conditioned in ACSF at 37 °C ($E'_{lr}$ = 130 GPa, $E'_{tr}$ = 5 GPa, $E'_S$ = 11 MPa, $G'_r$ = 1.77 GPa, $G'_S$ = 3.9 MPa, $\nu_r$ = 0.3, $\nu_s$ = 0.44).[72] (b) Tensile storage moduli ($E'$) of neat PVOH and PVOH/c-CNC nanocomposites as a function of CNC content in the dry state at 100 °C (■), and ACSF-swollen after immersion in ACSF at 37 °C for 1 week (▲). The solid line shows values predicted by the percolation model ($E'_r$ = 10 GPa). The dotted line shows the prediction by the Halpin−Kardos model for samples conditioned in ACSF at 37 °C ($E'_{lr}$ = 130 GPa, $E'_{tr}$ = 5 GPa, $E'_S$ = 1.44 MPa, $G'_r$ = 1.77 GPa, $G'_S$ = 0.5 MPa, $\nu_r$ = 0.3, $\nu_s$ = 0.44).[72] Because of solvent uptake the volume fraction of CNCs in ACSF-swollen samples is lower than in the dry state. Data points represent averages of $N$ = 3−6 measurements ± s.d.

and that the processing temperature of PVOH affects the permeability of the material and thereby the potential for water uptake.[70] Indeed, the swelling characteristics of the materials studied here were found to be strongly dependent on the temperature used for compression-molding, but not the type or content of CNCs. Neat PVOH and PVOH/t-CNC nanocomposite films processed at 150 °C exhibit ∼40% w/w swelling, whereas neat PVOH films and PVOH/c-CNC nanocomposites processed at 120 °C exhibit approximately ∼120% w/w swelling (Figure 4), regardless of the CNC content. The results indicate that the water uptake of the

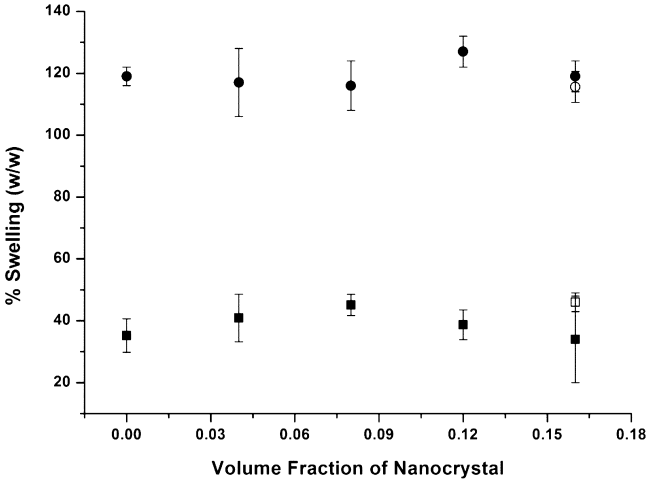


**Figure 4.** Swelling of PVOH/t-CNC nanocomposites compression-molded at 150 °C (■), PVOH/c-CNC nanocomposites compression-molded at 120 °C (●), a PVOH/t-CNC nanocomposite compression-molded at 120 °C (○), and a PVOH/c-CNC nanocomposite compression-molded at 150 °C (□) as a function of CNC content, after the samples were immersed in ACSF at 37 °C for 1 day. Data represent averages of $N$ = 3 measurements ± s.d.

PVOH/CNC nanocomposites is reduced by heat-treatment, likely on account of heat-induced cross-linking.[71] The conclusion that the processing temperature is the primary factor for the swelling behavior was further supported by swelling PVOH/c-CNC nanocomposites, which were processed at 150 °C, and PVOH/t-CNC nanocomposites, which were processed at 120 °C (Figure 4). Compared to the other nanocomposites, these samples exhibited swelling that was consistent with their processing temperature rather than the type of CNC. Swelling experiments in ACSF were extended over the course of two months to investigate the possible changes that might occur during prolonged biological implantation of the material (Table 4). The data show that for the PVOH/t-CNC nanocomposites processed at 150 °C equilibrium swelling is reached within 24 h and that these materials do not degrade over the course of two months. Similarly, PVOH/c-CNC nanocomposite films reached an equilibrated swelling within 24 h and maintained their integrity for at least one week. A comparison of the swelling data of the present PVOH/t-CNC and the previously investigated PVAc/t-CNC nanocomposites[30] shows that the PVOH-based nanocomposites swell much less than their PVAc-based counterparts. For instance, the PVAc/t-CNC nanocomposites comprising 16.5% v/v t-CNCs displayed a degree of swelling of ∼80%, while the PVOH/t-CNC nanocomposites shows ∼40% w/w of swelling with 16% v/v CNCs.

**Mechanical Properties of ACSF-Swollen Nanocomposites.** The mechanical properties of ACSF-swollen PVOH/CNC nanocomposites were determined by DMA using a submersion clamp setup, which allowed the samples to be immersed in ACSF during the measurements. Neat PVOH films softened substantially upon submersion in ACSF for one week and exhibited mechanical properties that appear to be correlated with their swelling behavior. Neat PVOH films processed at 150 °C displayed a change in $E'$ from ∼7.3 GPa (dry) to ∼11 MPa (ACSF-swollen), whereas $E'$ for neat PVOH films processed at 120 °C changed from 7.0 GPa to ∼1 MPa. The ACSF-swollen PVOH/t-CNC nanocomposites display an

Table 4. Swelling Data of Neat PVOH and PVOH/t-CNC Nanocomposites at 37 °C in ACSF as a Function of t-CNC Content[a]

| sample | t-CNC content (% v/v) | after 1 day (% w/w) | after 3 days (% w/w) | after 1 week (% w/w) | after 1 month (% w/w) | after 2 months (% w/w) |
|---|---|---|---|---|---|---|
| neat PVOH | | 35 ± 5 | 43 ± 4 | 38 ± 2 | 43 ± 4 | 45 ± 6 |
| PVOH/t-CNC | 4 | 41 ± 8 | 40 ± 6 | 48 ± 2 | 37 ± 8 | 50 ± 3 |
| | 8 | 45 ± 3 | 44 ± 7 | 42 ± 5 | 47 ± 9 | 48 ± 6 |
| | 12 | 39 ± 5 | 46 ± 9 | 37 ± 5 | 36 ± 5 | 46 ± 8 |
| | 16 | 34 ± 1 | 42 ± 3 | 40 ± 8 | 42 ± 5 | 41 ± 2 |

[a]Data represent averages ($N$ = 3) ± s.d.

$E'$ that is higher than of the neat PVOH films (Figure 5a and Figure S8 in the Supporting Information), but considerably

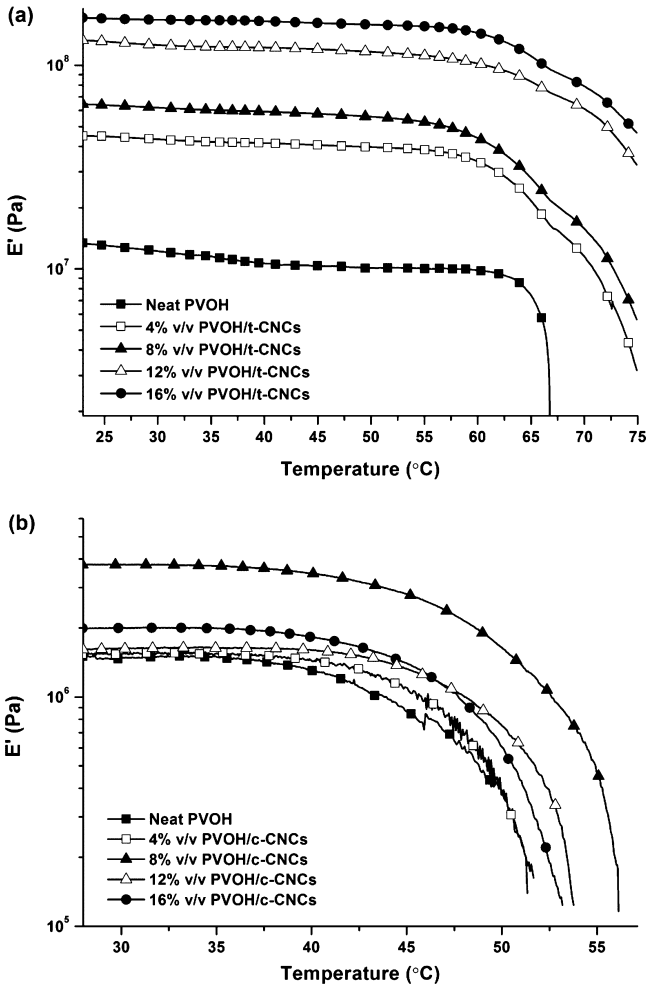


Figure 5. Dynamic mechanical analysis (DMA) data of ACSF-swollen films of (a) neat PVOH and PVOH/t-CNC nanocomposites and (b) PVOH/c-CNC nanocomposites as a function of temperature and CNC content after immersion in ACSF at 37 °C for 1 week.

lower than that of the corresponding materials in the dry state. For example, $E'$ of the material comprising 16% v/v t-CNCs dropped from 13.7 GPa (dry, RT) to ∼160 MPa (ACSF-swollen at 37 °C). The data in Figure 3 and Table 2 show that the switching is reversible and that ACSF exposure for 1 week and 1 month has the same effect. Moreover, the data in Figure 3a show that the relation between $E'$ of the ACSF-swollen PVOH/t-CNC nanocomposites and the t-CNC content is fairly well described by the Halpin−Kardos model, whose application to the modeling of CNC-based nanocomposites has been reported elsewhere.[29,30] Parameters used for the modeling (see caption to Figure 3) were taken from ref 72, except $E'_S$ of 11 and 1.44 MPa for materials processed at 150 and 120 °C, respectively, which were measured by DMA. The fact that the model underestimates $E'$ suggests that the CNC−CNC and perhaps also CNC−matrix interactions are reduced upon swelling with ACSF but, perhaps on account to the abundance of hydroxyl groups on the matrix polymer and the CNCs that can interact with water, not entirely switched off. All of the ACSF-swollen samples show a significant drop of $E'$ at ∼60 °C. Since this temperature is below the $T_g$ of the plasticized PVOH and far below the $T_m$ of the matrix (∼220 °C), we speculate that this transition is related to the dissolution of the matrix.

The ACSF-swollen PVOH and PVOH/c-CNC films, which were processed at 120 °C and display considerably more swelling than the above-discussed t-CNC-based materials, exhibit an $E'$ of 1−4 MPa at 37 °C (Figures 3b and 5b, Table 2). Because of the rather low modulus, these measurements feature a significant error, and it is therefore not possible to draw a firm conclusion about how the nanocomposite composition affects the modulus of the ACSF-swollen materials. The fact that the ACSF-induced mechanical switching was very significant and the finding that similar values were observed for both the neat PVOH and the nanocomposites suggest that the mechanical properties of these materials were largely governed by the swollen polymer matrix, supporting the notion that the water effectively reduced interactions between the CNCs and interrupted their continuous reinforcing network.

To further probe the influence of the processing temperature on the mechanical switching, the tensile storage moduli ($E'$) of nanocomposites with 16% v/v t-CNCs that had been compression-molded at 120 and 150 °C were compared (Table 2). It was found that the $E'$ of PVOH/t-CNC films processed at 150 °C, switched from 13.7 GPa (dry, RT) to 164 MPa (ACSF-swollen at 37 °C), whereas the material processed at 120 °C switched from 12.3 GPa to 60 MPa (Figure S9 in the Supporting Information). A similar result, was observed for the ACSF-swollen PVOH/c-CNC films, which if processed at 150 °C exhibited an $E'$ of 13 MPa at 37 °C, while the same composition processed at 120 °C, showed an $E'$ of 2 MPa at 37 °C (Figure S10 in the Supporting Information). A lower processing temperature therefore not only influences the mechanical properties of the materials in the dry state, but also reduces $E'$ of the ACSF-swollen state considerably. While the PVOH/c-CNC films processed at 150 °C show some yellowing, their dry-state mechanical properties are largely comparable to those of the material processed at 120 °C, and (on account of less swelling) a higher modulus in the soft state is achieved, suggesting that whatever effect is responsible for the yellowing, it is not negatively impacting the material's mechanical characteristics. Thus, it appears that if PVOH is

used as a matrix, not only the CNC type and content but also the processing temperature can be used to tailor the mechanical contrast of CNCs-based, water-responsive, mechanically adaptive nanocomposites.

## CONCLUSIONS

In summary, water-responsive, mechanically adaptive nanocomposites based on PVOH and t-CNCs or c-CNCs offer an initial stiffness that is significantly higher than that of previous generations of such responsive materials. The use of PVOH as a matrix polymer into which CNCs are incorporated proved useful for several reasons. The tensile storage moduli of PVOH/CNC nanocomposites were, in both the glassy and rubbery regime, significantly higher than those of comparable nanocomposites. It appears that in addition to CNC−CNC interactions, polymer−CNC interactions, which could be promoted by the strong propensity of PVOH to form hydrogen bonds and provide a compatible polymer−filler interface, are a significant factor in this context. Another significant factor is the possibility of controlling the swelling characteristics of the PVOH matrix, and therewith the properties of water- or ACSF-swollen nanocomposites, via the processing conditions. Using this tool, the switching "contrast" of the t-CNC-based nanocomposites upon exposure to ACSF could be varied between a 90-fold to a 200-fold modulus reduction. The results suggest that other ranges can be dialed in via the processing temperature, which (in relative terms) affects mainly the soft state. Although not as stiff initially in the dry state, PVOH/c-CNC nanocomposites exhibit a larger mechanical contrast (up to 900-fold), as they soften much more than the t-CNC-based materials. This effect is related to the lower reinforcing power of c-CNCs. Despite the fact that decomposition of the c-CNC-containing materials starts around 150 °C, the nanocomposites maintain useful mechanical properties. Therefore, one could envision employing a higher processing temperature for PVOH/c-CNC nanocomposites to further increase the stiffness of the water-swollen state. Overall, we have demonstrated that varying the CNC type and concentration and the processing temperature allows one to tailor the mechanical properties of "hard" and "soft" state over a broad range. The hitherto unavailable contrasts accessible by the new materials make them potentially useful as substrates for neural prosthetic devices. Ongoing work in vivo studies seek to quantify the potential benefits of these mechanically switchable materials as basis for adaptive neural interfaces.

## ASSOCIATED CONTENT

### Supporting Information

Conductometric titration curves of t-CNCs and c-CNCs; TEM images of lyophilized t-CNCs, c-CNCs, and spray-dried c-CNCs; topographic AFM images of CNCs; photograph of solution-cast PVOH/c-CNC nanocomposites processed at 150 and 120 °C; DSC thermograms of a neat PVOH film and PVOH/CNC nanocomposites; stress−strain curves of PVOH/CNC nanocomposites as function of CNC content; DMA data of ACSF-swollen films of neat PVOH and PVOH/t-CNC nanocomposites after immersion in ACSF at 37 °C for 1 month; DMA data of ACSF-swollen 16% v/v PVOH/CNC nanocomposites after immersion in ACSF at 37 °C for 1 day; photograph of t-CNC aerogel prepared by lyophilization of aqueous dispersion. This material is available free of charge via the Internet at http://pubs.acs.org.

## AUTHOR INFORMATION

### Corresponding Author

*E-mail: christoph.weder@unifr.ch.

### Notes

The authors declare no competing financial interest.

## ACKNOWLEDGMENTS

The authors gratefully acknowledge financial support received from the Swiss National Science Foundation (NRP 62: Smart Materials, Nr. 406240_126046) and Fresenius-Kabi.

## REFERENCES

(1) *Handbook of Stimuli-Responsive Materials*, 1 ed.; Urban, M. W., Ed.; Wiley-VCH: Weinheim, Germany, 2011.
(2) *Intelligent Materials*, 1 ed.; Shahinpoor, M., Schneider, H. J., Eds.; RSC Publishing: London, 2007.
(3) Stuart, M. A. C.; Huck, W. T. S.; Genzer, J.; Muller, M.; Ober, C.; Stamm, M.; Sukhorukov, G. B.; Szleifer, I.; Tsukruk, V. V.; Urban, M.; Winnik, F.; Zauscher, S.; Luzinov, I.; Minko, S. *Nat. Mater.* **2010**, *9*, 101−113.
(4) Qiu, Y.; Park, K. *Adv. Drug Delivery Rev.* **2001**, *53*, 321−339.
(5) Alarcon, C. d. l. H.; Pennadam, S.; Alexander, C. *Chem. Soc. Rev.* **2005**, *34*, 276−285.
(6) Kim, Y. J.; Choi, S.; Koh, J. J.; Lee, M.; Ko, K. S.; Kim, S. W. *Pharm. Res.* **2001**, *18*, 548−550.
(7) Rosengart, A. J.; Kaminski, M. D.; Chen, H. T.; Caviness, P. L.; Ebner, A. D.; Ritter, J. A. *J. Magn. Magn. Mater.* **2005**, *293*, 633−638.
(8) Needham, D.; Dewhirst, M. W. *Adv. Drug Delivery Rev.* **2001**, *53*, 285−305.
(9) Peppas, N. A.; Hilt, J. Z.; Khademhosseini, A.; Langer, R. *Adv. Mater.* **2006**, *18*, 1345−1360.
(10) Bachelder, E. M.; Beaudette, T. T.; Broaders, K. E.; Dashe, J.; Frechet, J. M. J. *J. Am. Chem. Soc.* **2008**, *130*, 10494−10495.
(11) Chen, F. M.; Zhao, Y. M.; Sun, H. H.; Jin, T.; Wang, Q. T.; Zhou, W.; Wu, Z. F.; Jin, Y. *J. Controlled Release* **2007**, *118*, 65−77.
(12) Yang, J.; Yamato, M.; Kohno, C.; Nishimoto, A.; Sekine, H.; Fukai, F.; Okano, T. *Biomaterials* **2005**, *26*, 6415−6422.
(13) White, S. R.; Sottos, N. R.; Geubelle, P. H.; Moore, J. S.; Kessler, M. R.; Sriram, S. R.; Brown, E. N.; Viswanathan, S. *Nature* **2001**, *409*, 794−797.
(14) Cho, S. H.; Andersson, H. M.; White, S. R.; Sottos, N. R.; Braun, P. V. *Adv. Mater.* **2006**, *18*, 997−1000.
(15) Kwon, O. H.; Kikuchi, A.; Yamato, M.; Sakurai, Y.; Okano, T. *J. Biomed. Mater. Res.* **2000**, *50*, 82−89.
(16) Lee, H.; Park, T. G. *Biotechnol. Prog.* **1998**, *14*, 508−516.
(17) Pelrine, R.; Kornbluh, R.; Pei, Q. B.; Joseph, J. *Science* **2000**, *287*, 836−839.
(18) Ebron, V. H.; Yang, Z. W.; Seyer, D. J.; Kozlov, M. E.; Oh, J. Y.; Xie, H.; Razal, J.; Hall, L. J.; Ferraris, J. P.; MacDiarmid, A. G.; Baughman, R. H. *Science* **2006**, *311*, 1580−1583.
(19) Hsu, L.; Weder, C.; Rowan, S. J. *J. Mater. Chem.* **2011**, *21*, 2812−2822.
(20) Shanmuganathan, K.; Capadona, J. R.; Rowan, S. J.; Weder, C. *Prog. Polym. Sci.* **2010**, *35*, 212−222.
(21) Stone, D. A.; Wanasekara, N. D.; Jones, D. H.; Wheeler, N. R.; Wilusz, E.; Zukas, W.; Wnek, G. E.; Korley, L. T. J. *ACS Macro Lett.* **2011**, *1*, 80−83.
(22) Eichhorn, S. J.; Dufresne, A.; Aranguren, M.; Marcovich, N. E.; Capadona, J. R.; Rowan, S. J.; Weder, C.; Thielemans, W.; Roman, M.; Renneckar, S.; Gindl, W.; Veigel, S.; Keckes, J.; Yano, H.; Abe, K.; Nogi, M.; Nakagaito, A. N.; Mangalam, A.; Simonsen, J.; Benight, A. S.; Bismarck, A.; Berglund, L. A.; Peijs, T. *J. Mater. Sci.* **2010**, *45*, 1−33.
(23) Habibi, Y.; Lucia, L. A.; Rojas, O. J. *Chem. Rev.* **2010**, *110*, 3479−3500.
(24) Eichhorn, S. J. *Soft Matter* **2011**, *7*, 303−315.
(25) Samir, M. A. S. A.; Alloin, F.; Dufresne, A. *Biomacromolecules* **2005**, *6*, 612−626.

(26) Favier, V.; Chanzy, H.; Cavaille, J. Y. *Macromolecules* **1995**, *28*, 6365−6367.
(27) Favier, V.; Canova, G. R.; Cavaillé, J. Y.; Chanzy, H.; Dufresne, A.; Gauthier, C. *Polym. Adv. Technol.* **1995**, *6*, 351−355.
(28) Capadona, J. R.; Shanmuganathan, K.; Tyler, D. J.; Rowan, S. J.; Weder, C. *Science* **2008**, *319*, 1370−1374.
(29) Shanmuganathan, K.; Capadona, J. R.; Rowan, S. J.; Weder, C. *J. Mater. Chem.* **2010**, *20*, 180−186.
(30) Shanmuganathan, K.; Capadona, J. R.; Rowan, S. J.; Weder, C. *ACS Appl. Mater. Interfaces* **2010**, *2*, 165−174.
(31) Mendez, J.; Annamalai, P. K.; Eichhorn, S. J.; Rusli, R.; Rowan, S. J.; Foster, E. J.; Weder, C. *Macromolecules* **2011**, *44*, 6827−6835.
(32) Way, A. E.; Hsu, L.; Shanmuganathan, K.; Weder, C.; Rowan, S. J. *ACS Macro Letters* **2012**, *1*, 1001−1006.
(33) Dagnon, K. L.; Shanmuganathan, K.; Weder, C.; Rowan, S. J. *Macromolecules* **2012**, *45*, 4707−4715.
(34) Shin, M. K.; Spinks, G. M.; Shin, S. R.; Kim, S. I.; Kim, S. J. *Adv. Mater.* **2009**, *21*, 1712−1715.
(35) Schmidt, D. J.; Cebeci, F. C.; Kalcioglu, Z. I.; Wyman, S. G.; Ortiz, C.; Van Vliet, K. J.; Hammond, P. T. *ACS Nano* **2009**, *3*, 2207−2216.
(36) Spinks, G. M.; Mottaghitalab, V.; Bahrami-Samani, M.; Whitten, P. G.; Wallace, G. G. *Adv. Mater.* **2006**, *18*, 637−640.
(37) Capadona, J. R.; Van Den Berg, O.; Capadona, L. A.; Schroeter, M.; Rowan, S. J.; Tyler, D. J.; Weder, C. *Nat. Nanotechnol.* **2007**, *2*, 765−769.
(38) Hess, A. E.; Capadona, J. R.; Shanmuganathan, K.; Hsu, L.; Rowan, S. J.; Weder, C.; Tyler, D. J.; Zorman, C. A. *J. Micromech. Microeng.* **2011**, *21*, 054009.
(39) Harris, J. P.; Hess, A. E.; Rowan, S. J.; Weder, C.; Zorman, C. A.; Tyler, D. J.; Capadona, J. R. *J. Neural Eng.* **2011**, *8*, 040610.
(40) Capadona, J. R.; Tyler, D. J.; Zorman, C. A.; Rowan, S. J.; Weder, C. *MRS Bull.* **2012**, *37*, 581−589.
(41) Harris, J. P.; Capadona, J. R.; Miller, R. H.; Healy, B. C.; Shanmuganathan, K.; Rowan, S. J.; Weder, C.; Tyler, D. J. *J. Neural Eng.* **2011**, *8*, 066011.
(42) Chiellini, E.; Cinelli, P.; Hieva, V. I.; Martera, M. *Biomacromolecules* **2008**, *9*, 1007−1013.
(43) Hyon, S. H.; Ikada, Y. Method of molding a polyvinyl alcohol contact lens. U.S. Patent 4874562, Oct 17, 1989.
(44) Lee, P. I. Production of borate cross-linked polyvinyl alcohol contact lenses. U.S. Patent 4559186, Dec 17, 1985.
(45) Janssen, R. A.; Lee, P. I.; Ajello, E. M. Preparation of stable polyvinyl alcohol hydrogel contact lens. U.S. Patent 5174929, Dec 29, 1992.
(46) Nectow, A. R.; Marra, K. G.; Kaplan, D. L. *Tissue Eng., Part B* **2012**, *18*, 40−50.
(47) Uddin, A. J.; Araki, J.; Gotoh, Y. *Polym. Int.* **2011**, *60*, 1230−1239.
(48) Uddin, A. J.; Araki, J.; Gotoh, Y. *Biomacromolecules* **2011**, *12*, 617−624.
(49) Paralikar, S. A.; Simonsen, J.; Lombardi, J. *J. Membr. Sci.* **2008**, *320*, 248−258.
(50) Roohani, M.; Habibi, Y.; Belgacem, N. M.; Ebrahim, G.; Karimi, A. N.; Dufresne, A. *Eur. Polym. J.* **2008**, *44*, 2489−2498.
(51) Lue, J.; Wang, T.; Drzal, L. T. *Composites, Part A* **2008**, *39*, 738−746.
(52) www.alzet.com/products/cfs_prep.php (accessed 08/04/2009).
(53) Sun, C. C. *J. Pharm. Sci.* **2005**, *94*, 2132−2134.
(54) Capadona, J. R.; Shanmuganathan, K.; Triftschuh, S.; Seidel, S.; Rowan, S. J.; Weder, C. *Biomacromolecules* **2009**, *10*, 712−716.
(55) Sturcova, A.; Davies, G. R.; Eichhorn, S. J. *Biomacromolecules* **2005**, *6*, 1055−1061.
(56) Rusli, R.; Eichhorn, S. J. *Appl. Phys. Lett.* **2008**, 93.
(57) van den Berg, O.; Capadona, J. R.; Weder, C. *Biomacromolecules* **2007**, *8*, 1353−1357.
(58) Roman, M.; Winter, W. T. *Biomacromolecules* **2004**, *5*, 1671−1677.
(59) Rosa, M. F.; Medeiros, E. S.; Malmonge, J. A.; Gregorski, K. S.; Wood, D. F.; Mattoso, L. H. C.; Glenn, G.; Orts, W. J.; Imam, S. H. *Carbohydr. Polym.* **2010**, *81*, 83−92.
(60) Alloin, F.; D'Aprea, A.; Kissi, N. E.; Dufresne, A.; Bossard, F. *Electrochim. Acta* **2010**, *55*, 5186−5194.
(61) Kropka, J. M.; Putz, K. W.; Pryamitsyn, V.; Ganesan, V.; Green, P. F. *Macromolecules* **2007**, *40*, 5424−5432.
(62) George, J.; Ramana, K. V.; Bawa, A. S.; Siddaramaiah. *Int. J. Biol. Macromol.* **2011**, *48*, 50−57.
(63) Johnsy, G.; Datta, K. K. R.; Sajeevkumar, V. A.; Sabapathy, S. N.; Bawa, A. S.; Eswaramoorthy, M. *ACS Appl. Mater. Interfaces* **2009**, *1*, 2796−2803.
(64) Zhang, Q.; Brumer, H.; Ågren, H.; Tu, Y. *Carbohydr. Res.* **2011**, *346*, 2595−2602.
(65) Liang, J. J.; Huang, Y.; Zhang, L.; Wang, Y.; Ma, Y. F.; Guo, T. Y.; Chen, Y. S. *Adv. Funct. Mater.* **2009**, *19*, 2297−2302.
(66) Liu, L. Q.; Barber, A. H.; Nuriel, S.; Wagner, H. D. *Adv. Funct. Mater.* **2005**, *15*, 975−980.
(67) Dufresne, A.; Vincendon, M. *Macromolecules* **2000**, *33*, 2998−3008.
(68) Morin, A.; Dufresne, A. *Macromolecules* **2002**, *35*, 2190−2199.
(69) Tang, L. M.; Weder, C. *ACS Appl. Mater. Interfaces* **2010**, *2*, 3396−3396.
(70) Lim, L. Y.; Wan, L. S. C. *Drug Dev. Ind. Pharm.* **1995**, *21*, 369−373.
(71) Sriupayo, J.; Supaphol, P.; Blackwell, J.; Rujiravanit, R. *Polymer* **2005**, *46*, 5637−5644.
(72) Hajji, P.; Cavaille, J. Y.; Favier, V.; Gauthier, C.; Vigier, G. *Polym. Compos.* **1996**, *17*, 612−619.
(73) Kubo, S.; Kadla, J. F. *Biomacromolecules* **2003**, *4*, 561−567.